Pergamon

Int. J. Heat Mass Transfer. Vol. 41, No. 1, pp. 209–218, 1998

Printed in Great Britain
0017-9310/98 $19.00+0.00

PII: S0017-9310(97)00107-5

Heat-transfer characteristics of magnetofluidized beds of pure and admixtures of magnetic and nonmagnetic particles

V. L. GANZHA† and S. C. SAXENA‡

Multiphase Reactor Research Laboratory, Department of Chemical Engineering (M/C 110), The University of Illinois at Chicago, 810 S. Clinton Street, Chicago, IL 60607-7000, U.S.A.

(*Received* 28 *August* 1996)

Abstract—The hydrodynamic behavior of an iron and iron-sand beds is investigated in the presence of an externally applied uniform magnetic field collinear with gas flow. In addition heat-transfer measurements from a horizontal electrically heated probe are conducted. The gas velocity is varied over a wide range to bring about different regimes for different magnetic-field intensity values in the range 0–9641 A m^{-1}. The minimum bubbling velocity and heat-transfer coefficient values are discussed and correlated. It is found that bed voidage and segregation of admixture components play a very important role in establishing the hydrodynamic and heat-transfer characteristics of the magnetofluidized beds. © 1997 Elsevier Science Ltd.

INTRODUCTION

The hydrodynamic structure of gas–solid fluidized beds has been explored in great detail by different experimental approaches such as direct tracking of bed particles, bed mixing studies, pressure-drop fluctuation history records, bubble dynamics, bed temperature distribution, heat-transfer etc., and different theoretical modeling considerations. Some 35 years ago, it was realized that a bed of magnetic particles exposed to an almost uniform magnetic field behaves under certain conditions somewhat similar to gas–solid fixed and fluidized beds under the influence of gravitational field only. Experiments on magnetic particle beds have revealed that different bed structural configurations are achieved depending upon the value of the superficial gas velocity (U_g), magnetic-field intensity (H), particle size (d_p) and density (ρ_s), and particle magnetic properties such as susceptibility (χ), and permeability (μ_M). The general understanding is that at a given H as U_g is increased, the bed exhibits the familiar fixed-bed behavior adequately described by Carman–Kozeny formulation; at $U_g \approx U_{mf}$, the bed does not exhibit the familiar properties of fluidized beds at incipient fluidization, but instead the bed expansion occurs as the magnetic particles arrange themselves along the magnetic lines of force. Bubbles appear at $U_g = U_{mb}$; and for $U_g > U_{mb}$, the bed behaves somewhat like a conventional bubbling fluidized bed. The significant characteristic properties of such a bed over the entire range of gas velocities are studied in terms of different fluidization regimes which are mentioned below.

The different fluidization regimes are: for $U_g < U_{mf}$, fixed-bed regime; $U_{mf} \leqslant U_g < U_{mb}$, magnetically stabilized regime (MSB); and for $U_g \geqslant U_{mb}$, magnetically stabilized fluidized-bed regime (MSFB) or partially stabilized-bed regime. If H is sufficiently large such that the interparticle forces are very strong, the frozen-bed regime may result. Detailed descriptions of magnetofluidized beds, their different characteristics, and their applications have been discussed recently in several review articles such as those of Sonolikar [1], Liu *et al.* [2] and Saxena *et al.* [3].

Few studies dealing with heat transfer from an immersed surface to magnetofluidized beds have been reported in the different regimes mentioned above. The pioneering work of Bologa and Syutkin [4] dealt with beds of iron particles of different sizes up to 500 μm, H up to 10,000 A m^{-1}, and at ambient conditions. A heater probe, 30 mm long and 18 mm in diameter, was used in a bed of 78 mm diameter in a vertical configuration at different heights. Neff and Rubinsky [5] reported h_w measurements for an iron-chilled shot bed of $d_p = 727$ μm for several H values up to about 3000 A m^{-1}, in a 8.89 cm diameter cylindrical bed equipped with a vertical flat heater at ambient conditions. Arnaldos *et al.* [6] determined h_w for pure magnetic materials, steel (350–420 μm) and nickel (250–400 μm) shots, and their admixtures with silica sand (630–890 μm), and an electrically heated vertical stainless-steel tube, 140 mm long and 6 mm outer diameter at ambient conditions. The bed was contained in a 70 mm stainless-steel column, and H was varied up to about 4000 A m^{-1}. Saxena *et al.* [3],

† Permanent address: Luikov Institute of Heat and Mass Transfer of Belarussian Academy of Sciences, 15 P. Brovka Street, Minsk 220072, Belarus.

‡ Author to whom correspondence should be addressed.

NOMENCLATURE

A bed cross-sectional area [m^2]
Ar Archimedes number
C numerical coefficient in equation (8)
d_M average particle diameter of magnetic powder [m]
d_p average particle diameter [m]
E_R potential energy density ratio
g acceleration due to gravity [m s^{-2}]
H magnetic-field intensity [A m^{-1}]
h_w heat-transfer coefficient [W m^{-2} · K^{-1}]
I electrical current [A]
k_g gas thermal conductivity [W (m · K)$^{-1}$]
k_p particle thermal conductivity [W (m · K)$^{-1}$]
K_{gp} a parameter defined by equation (9)
L height of either a bed section or total bed [m]
L_0 stagnant unfluidized bed height [m]
Nu Nusselt number
Pr Prandtl number
R_1, R_2, R_3 bridge arm resistors [Ohm]
Re Reynolds number
R_{pr} probe resistance [Ohm[
S_{pr} probe-surface area [m^2]
T_b bed temperature [K]
U_g superficial gas velocity [m s^{-1}]
U_{mb} superficial minimum bubbling gas velocity [m s^{-1}]
U_{mf} superficial minimum fluidization gas velocity [m s^{-1}]
V_p probe volume [m^3]
X_M mass fraction of iron in the bed, dimensionless.

Greek symbols
ΔP_b bed pressure drop [N m^{-2}]
ΔP_L pressure drop across a bed section of length L [N m^{-2}]
ε bed voidage
μ_b bed magnetic permeability [H m^{-1}]
μ_M magnetic permeability of magnetizable particles [H m^{-1}]
μ_0 magnetic permeability of free space [H m^{-1}]
ν kinetic gas viscosity [m^2 s^{-1}]
ρ_g gas density [kg m^{-3}]
ρ_M density of iron particles [kg m^{-3}]
ρ_N density of sand particles [kg m^{-3}]
ρ_s density of an admixture of iron and sand particles [kg m^{-3}]
χ magnetic susceptibility.

Acronyms
MSB magnetically stabilized bed
MSBA magnetically stabilized bed of admixture particles
MSFB magnetically stabilized fluidized bed.

Qian and Saxena [7], and Saxena and Dewan [8] have reported h_w values at ambient conditions for horizontal, electrically heated, probes of 16.3 mm and 24.1 mm diameters and for beds of iron shots of 733 and 1511 μm, and for maximum H values up to about 20,000 A m^{-1}.

In view of the promising applications of magnetically stabilized beds of admixtures (MSBA) of magnetic and nonmagnetic particles and our limited knowledge of such systems, measurements have been conducted with an admixture of sand and iron shots at ambient conditions contained in a bed of 102 mm column. H is varied from 0 to about 10,000 A m^{-1}, and U_g is varied over a large range covering different fluidization regimes mentioned above. These results are presented in this article. The only work of h_w measurements with admixtures of magnetic and nonmagnetic particles so far reported is that of Arnaldos *et al.* [6].

EXPERIMENTAL FACILITY AND PROCEDURE

The experimental equipment and their design details are very similar to those reported by Saxena *et al.* [3]. The facility is moved to a different location and has been tested with some of the components redesigned and refabricated [9]. It consists of an air supply system, a fluidization column, and Helmholtz electromagnet with an HP6274B DC power supply, an off-gas cleaning system, and three DP cells connected to a Hewlett-Packard data acquisition system. A horizontal heat-transfer probe in the bed is employed to measure the bed to surface heat-transfer coefficients as a function of superficial gas velocity, U_g, and magnetic-field intensity, H, applied collinear to the gas velocity flow vector. The experimental arrangement is briefly described below.

A 45 kW single-stage, positive displacement, air-cooled and flood-lubricated rotary screw type compressor is used to supply compressed, dried and filtered air. The fluidization column is fabricated from a 12.5 mm thick transparent Plexiglas pipe with an internal diameter of 0.102 m, and comprises of a 0.21 m long calming section, and bed and freeboard sections with a combined height of 3.5 m. The calming and bed gas distributor plates are suitably designed perforated Plexiglas plates having adequate pressure drops. These are measured by four pressure probes

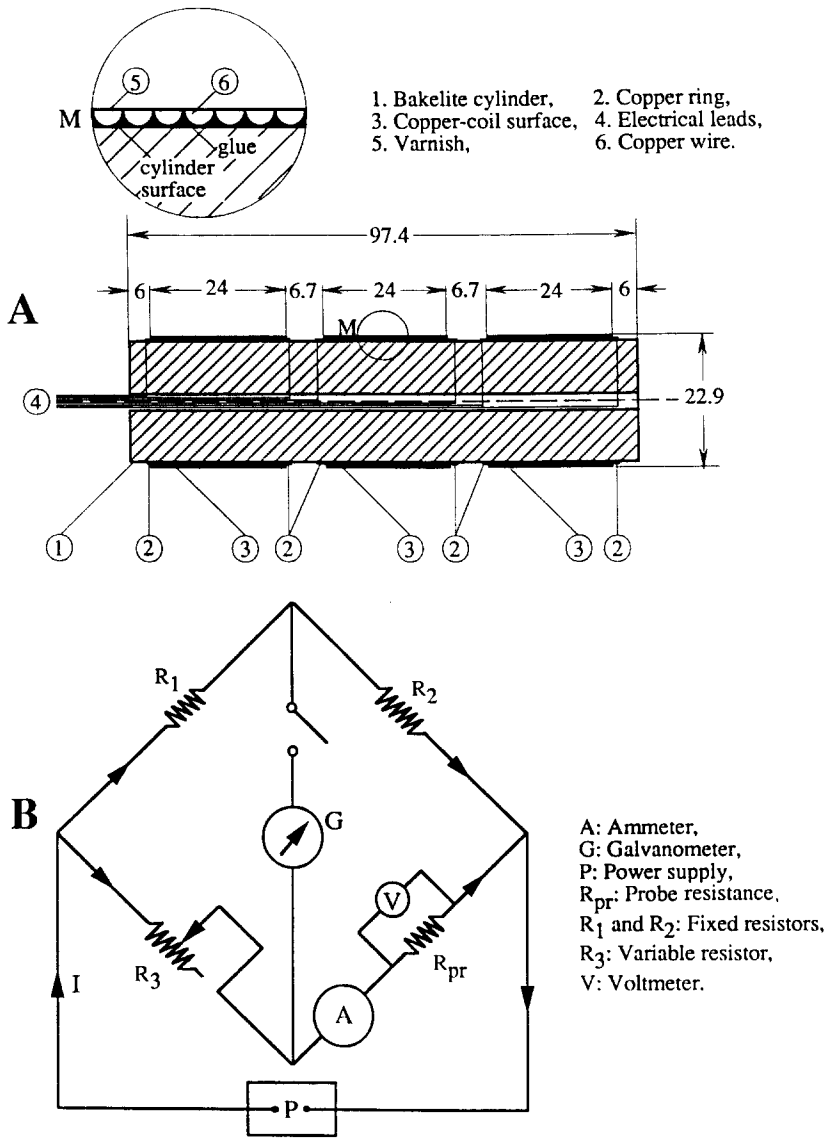

Fig. 1. (a) Schematic of heater heat-transfer probe. All dimensions are in mm. (b) The electrical circuit.

located at 6, 66.1, 142.3 and 332.8 mm above the bed distributor plate and connected to DP cells.

The two Helmholtz electromagnet coils have an inner diameter of 0.358 m and are separated by a distance of 0.171 m. The coils are designed for a maximum operation at 60 V and 15 A to produce a constant magnetic-field of 27,137 A m^{-1}. The detailed measurements of Wu *et al.* [10] revealed that variations in a horizontal plane are quite small, except for $H > 21{,}000$ A m^{-1} where variations in the range 4–6% occur at several positions. Variations in the z-direction occur even at relatively lower H values, about 10,000 A m^{-1}, in the range of about 5%.

A heat-transfer probe heater is designed and these details are shown in Fig. 1(a). It is made by winding insulated 80 μm copper wire over a Bakelite rod, about 22 mm in diameter, and having poor thermal and electrical conducting properties. The tightly wound copper coil is held in position by glue and is machined to a depth of one wire radius, and then finished with a coat of an electric-resistant varnish. The average diameter of the finished heater probe surface is 22.9 mm. As is clear from Fig. 1(a), the probe with an overall length of 97.4 mm, comprises of three independent sections, each 24 mm long. These sections can be independently energized and are separated from each other by about 6.7 mm. The ends of the heater wires are soldered to copper rings which are pressed on to the rod. The current leads are also connected to these rings. This design enables the measurement of h_w in a horizontal plane, but in three different regions which may be particularly valuable in the interpretation of the hydrodynamic behavior of the bed. The probe can also be installed in a vertical configuration to investigate the thermal behavior in a vertical direction. For the present measurements, the

probe is installed in the bed with its axis at a distance of 47 mm above the distributor plate. The bed temperature is measured by a thermocouple probe connected to a direct reading temperature device, numatron, in the vicinity of the probe, about 66 mm above the distributor plate.

The heat-transfer probe constitutes an arm of a bridge as shown in Fig. 1(b). R_1 and R_2 are fixed resistors having resistance values of about 250 and 2500 Ohm, respectively. The D.C. power supply (P) is a Hewlett-Packard programmable model HP-IB series having a range of 0–120 V, and 0–1.5 A. The probe is calibrated while immersed in a thermostat at 323.2 K and the resistor R_3 is adjusted to get the bridge balance. This is obtained for a very low value of current so that the probe is at the bath temperature. The probe is then installed in the bed.

While measuring the heat-transfer coefficient, the power supplied to the bridge is varied to get the bridge balance. The power provided to the probe is $I^2R_2^2R_{pr}(R_2+R_{pr})^{-2}$. Hence

$$h_w = \frac{I^2R_2^2R_{pr}}{(R_2+R_{pr})^2(323.2-T_b)S_{pr}} \quad (1)$$

where $S_{pr} = 0.001726$ m^2. This relationship is used for computing h_w for an end section to which all the measurements reported here refer. R_{pr} is determined by measuring directly the current in the probe arm and voltage across the probe during calibration at 323.2 K. As an alternative to equation (1), one could employ the probe arm current directly.

The test bed materials employed are sand and iron shot powders which are sieved to obtain samples in the narrow size range of 1.00–1.18 mm, with an average diameter of 1.086 mm. Equal volumes of sand and iron shots are used to prepare an admixture with the mass fractions of 0.25 and 0.75 for sand and iron shots, respectively. This admixture is put in the bed with a slumped height of about 71 mm and is thoroughly mixed by passing air at high superficial velocity. The heat-transfer measurements for pure materials and this admixture bed are taken at several values of magnetic-field intensity (H) and at each H for various values of increasing air velocity, U_g, over a wide range. Several sets of data are also taken for decreasing U_g. Simultaneously, the pressure-drop and bed height measurements are taken to obtain bed voidage values from the following relations:

$$\varepsilon_b = 1-(A\,\Delta P_L)[(AL-V_p)g(\rho_s-\rho_g)]^{-1} \quad (2)$$

and

$$\rho_s = [(X_M/\rho_M)+\{(1-X_M)/\rho_N\}]^{-1}. \quad (3)$$

Here ΔP_L is the pressure drop across either a bed section of height L or the entire bed for $U_g > U_{mf}$, V_p is the probe volume, X_M is the mass fraction of iron in the admixture, and ρ_M and ρ_N are the densities of iron and sand particles, respectively.

RESULTS AND DISCUSSION

Bed pressure drops, ΔP_b, are measured as a function of increasing and decreasing U_g for iron shots (slumped bed height = 71 mm) and sand particles (slumped bed height = 108 mm) in the absence of magnetic field. The results are displayed in Fig. 2. The minimum fluidization velocities (U_{mf}) are: 0.58 m s^{-1} for sand bed, and 1.26 m s^{-1} for the iron bed. Different U_{mf} values for the two admixture components can cause particle segregation at U_g values greater than U_{mf}. However, the fluidization behavior of such systems is likely to be of great practical significance. Equal sizes for the two components of the admixture bed will require discrete and distinct spatial movement of the particles while bringing about magnetic stabilization of particle ordering under the influence of H.

Variations of ΔP_b with decreasing U_g values for five H values are shown in Fig. 3 for the iron bed. These plots are employed to determine U_{mb} and the principle behind this procedure is explained by Saxena and Shrivastava [11]. The experimental U_{mb} values as a

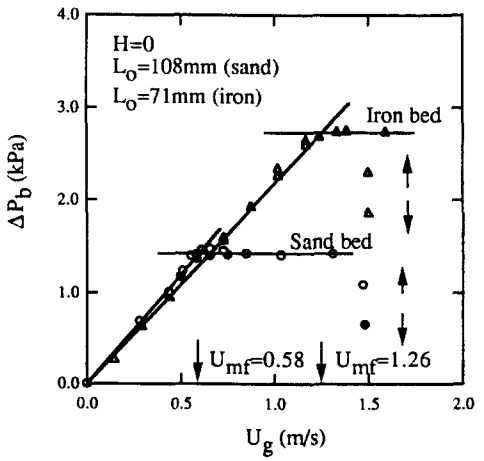

Fig. 2. Variation of ΔP_b with increasing (↑) and decreasing (↓) U_g.

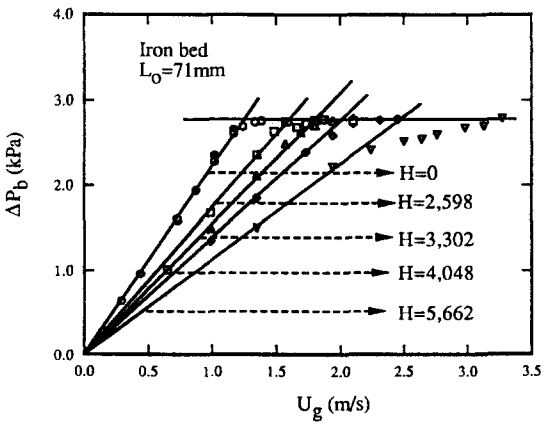

Fig. 3. Variation of ΔP_b with decreasing U_g at different H (A m^{-1}).

Table 1. Experimental and calculated U_{mb} values for the iron bed

H [A m^{-1}]	0	2598	3302	4048	5662
U_{mb} (exp.) [m s^{-1}]	1.26	1.56	1.76	1.95	2.21
U_{mb} (cal.) [m s^{-1}]	—	1.51	1.66	1.83	2.06

function of H are listed in Table 1 and it is to be noted that U_{mb} is always greater than U_{mf} and U_{mb} increases with an increase in H. This, of course, is as expected and is indeed the advantage of magnetically stabilized beds which give greater gas flow through the bed without causing bubbling as compared to unstabilized beds.

U_{mb} values are also calculated according to the following expression derived by Ganzha and Saxena [12]:

$$U_{mb} = U_{mf} + 0.0015(\nu/d_p)Ar^{0.81}E_R^{0.59} \quad (4)$$

where

$$Ar = gd_p^3(\rho_s - \rho_g)/\rho_g\nu^2 \quad (5)$$

$$E_R = (3/2)\mu_b X_M H^2/\boldsymbol{g}d_M\rho_M \quad (6)$$

and

$$\mu_b = \varepsilon\mu_0 + (1-\varepsilon)\mu_0 \exp(0.03\mu_M H X_M). \quad (7)$$

The calculated U_{mb} values for the iron bed are also listed in Table 1 and are in good agreement with the experimental values. The qualitative trend of disagreement between the experimental and calculated U_{mb} values is a bit puzzling, but is of no concern in view of its small magnitude.

The data for the admixture bed similar to that of Fig. 3 are presented in Fig. 4 together with voidage values obtained from equations (2) and (3). These bed voidage values refer to the bed section confined between 6 and 66 mm above the distributor plate and to the stabilized, and partially stabilized, bed regimes. In all cases ε exhibits an increase with an increase in U_g. This U_g range covers three distinct hydrodynamic states of the bed as established by visual observations. These are: no segregation of bed particles, segregation with sand iron particles preferentially accumulating in the top and bottom sections of the bed, respectively, and good back mixing of the bed particles. Gross ε measurements of Fig. 4 are incapable of discriminating these states and no quantitative criteria can be formulated for the delineation of these states. More detailed and careful bed sectional voidage measurements are needed to accomplish this goal. With an increase of H, it was observed that bed particle segregation commenced at U_g values closer to U_{mb}.

Experimental

U_{mb} experimental values as a function of H for the admixture bed are listed in Table 2 along with the corresponding calculated values from equations (4) to (7). Experimental U_{mb} values increase for this admixture bed with an increase in H similar to that for pure iron bed. This trend is also clearly exhibited in the computed values except the rate of increase is slower for $H \geqslant 6704$ A m^{-1}. The agreement between calculated and experimental values is considered good for H values up to 4686 A m^{-1}. The larger disagreement for $H \geqslant 6704$ A m^{-1} between the experimental and calculated U_{mb} values is attributed to the observed pronounced segregation of the two kinds of bed particles. Qualitatively, at these states the bed behaves more like a bed having a larger proportion of magnetic particles in the bed than the initial value due to segregation. It will imply that calculated values are greater than those listed in Table 2. This will improve the agreement between experimental and calculated U_{mb} values. Another significant trend in the U_{mb} values of Table 2 lies in the fact that as H is increased bed particles get magnetized and their hydrodynamic behavior changes. For example, it is known [13] that magnetized particles have a larger value of U_{mf} than when the particles are not magnetized. Of course in developing equation (4), the influence of interparticle forces is ignored.

The measured values of h_w for the pure sand bed as a function of U_g are reported in Fig. 5. The variation of h_w with U_g is qualitatively similar to that generally found for bubbling fluidized bed. h_w increases linearly with U_g in the fixed-bed regime, and acquires a maximum value and thereafter decreases slowly as U_g increases. Also shown in Fig. 5 are the ε values and these are consistent with the h_w variation with U_g.

h_w values for the pure iron bed as a function of U_g for six H values are graphed in Fig. 6. At each H, three heat-transfer regimes seem to exist. For $U_g < U_{mf}$, the fixed-bed regime prevails and h_w increases slowly with an increase in U_g. For U_g values between U_{mf} and U_{mb}, mean h_w values exhibit an increase with U_g of about the same magnitude as in the fixed-bed regime. However, for U_g values close to the U_{mb}, the increase is rapid for a range of U_g values. This will imply some particle movement in the magnetically stabilized regime for U_g values close to U_{mb}. This may be the result of several factors. U_{mb} may not be a sharply defined value and some bubble induced particle activity gets initiated before a mean U_{mb} value is reached. This is easily understandable for powders having a size range. Further, in this regime particle orientation and arrangement take place and for $U_g < U_{mb}$, it may be a somewhat quasi-steady-state process so that the system is in a state of dynamic equilibrium giving limited particle movement for U_g values greater than U_{mf} and close to U_{mb}, but $< U_{mb}$. For $U_g \geqslant U_{mb}$, the bubbling regime brings about extensive particle movement and h_w rapidly increases to achieve its maximum value similar to a conventional bubbling fluidized bed. This logical, but somewhat conjectured, hydrodynamical picture of magnetically fluidized bed is consistent with the findings at different H. At higher H values, the U_g range

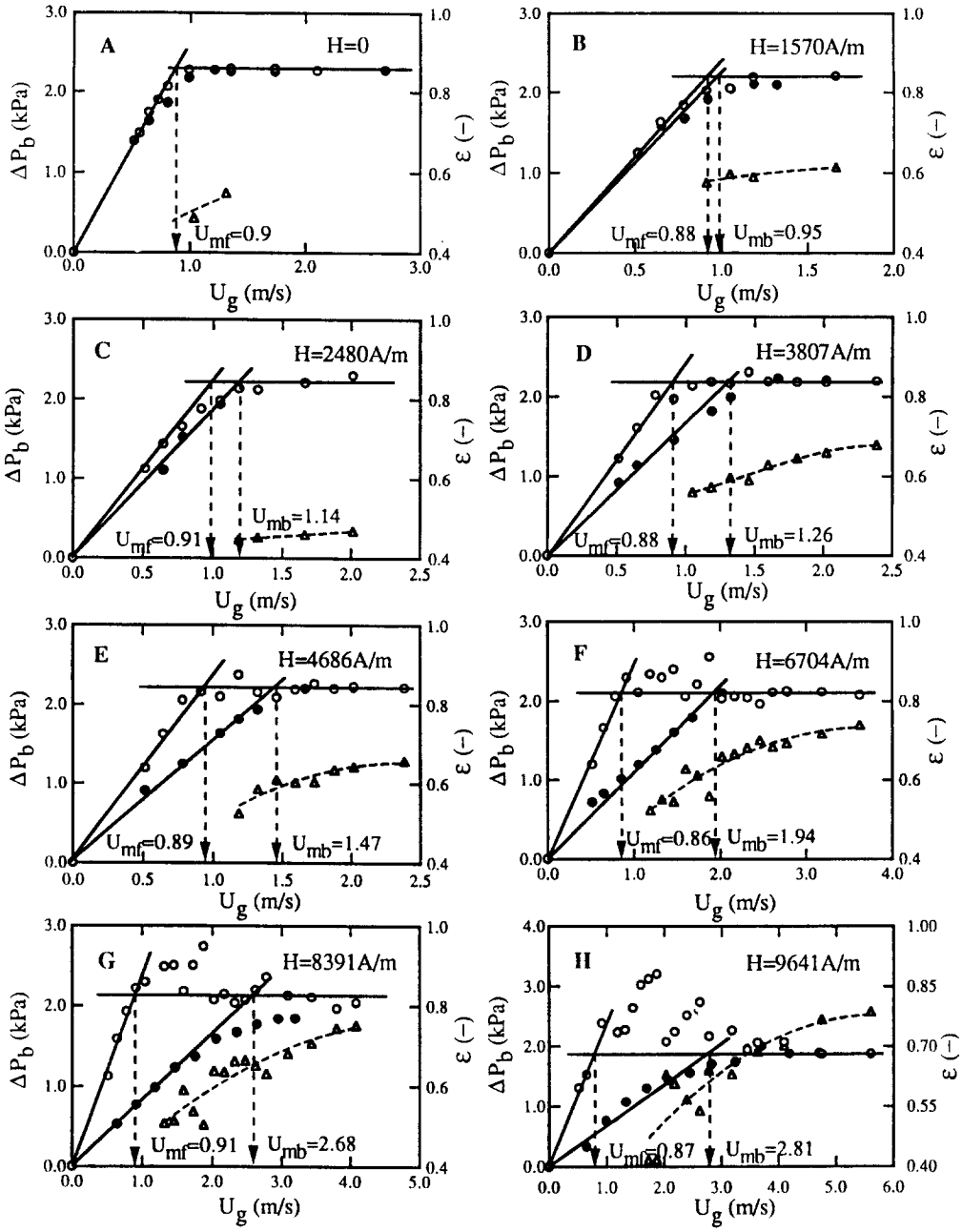

Fig. 4. Variation of ΔP_b and ε with increasing (○) and decreasing (●) U_g at different H for an admixture bed: sand (25%) and iron (75%).

bounded between U_{mf} and U_{mb} is comparatively large and h_w gradual increase with increasing U_g and sudden jump at U_{mb} are well exhibited.

The h_w variation in the stabilized region can be better understood by recalling that it is composed of two components, one is due to particle convection and the other due to gas convection. The voidage in the stabilized regime increases due to particle rearrangement in comparison to fixed-bed regime where the particle arrangement is random. Hence, in the stabilized regime, the interstitial gas velocity decreases causing the convective heat-transfer component to

Table 2. Experimental and calculated U_{mb} values for the admixture bed

H [A m^{-1}]	0	1570	2480	3807	4686	6704	8391	9641
U_{mb} (exp.) [m s^{-1}]	0.90	0.95	1.14	1.26	1.47	1.94	2.68	2.81
U_{mb} (cal.) [m s^{-1}]	—	0.98	1.03	1.13	1.22	1.36	1.51	1.72

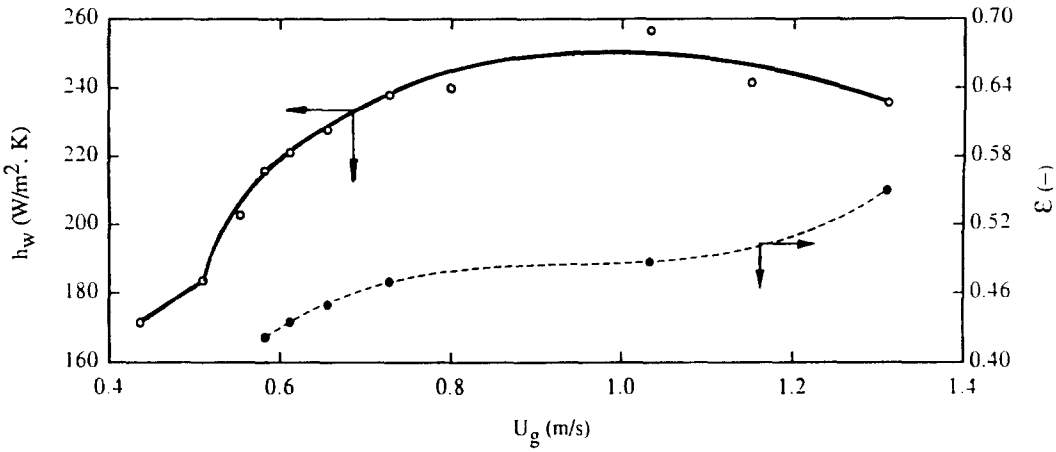

Fig. 5. Variation of h_w with increasing U_g for the sand bed.

decrease for the same increment in U_g as compared to the fixed-bed regime. The particle convective component of h_w as discussed above due to particle movement and/or arrangement gives a net increase to h_w. Further, it appears that the increase and decrease in particle and gas convective components respectively balance on the average so that the mean h_w values exhibit a somewhat similar increase with U_g in the stabilized regime as in the fixed-bed regime. It should also be noted that the jump in h_w near U_{mb} occurs in a narrower velocity band as H increases. This is because at higher H, the induced particle magnetization is larger and this enhances the interparticle force and hence particle immobility. These observations are in agreement with the earlier works [5, 6]. Further, it is very interesting to note in Fig. 6, that h_w decreases with an increase in H at values of U_g close to U_{mf}. This is also explained on a picture consistent with that given above, namely, the particle rearrangement or bed ordering degree increases with an increase in H. This increases ε_b relatively rapidly at larger H values and a resulting decrease in the interstitial gas velocity reduces h_w by a larger magnitude at greater H.

In Fig. 7, are presented the data for the admixture bed for nine H values as a function of U_g. In Fig. 7(a), the data for H values up to 4385 A m^{-1} are shown, and the behavior is similar to that of Fig. 6. The data clearly indicate the three heat-transfer regimes. The commencement of stabilized regime does occur at around U_g value of 0.9 m s^{-1}, which is the value of U_{mf} for the admixture bed (Fig. 4). In assessing the influence of H on h_w and the apparent qualitative difference in plots of Fig. 7(a, b), the contribution of inert (nonmagnetic) sand particles must be carefully taken into account. At higher H values (>5000 A m^{-1}), the magnetic particles form a sufficiently rigid structure through which the drag on sand particles pushes them to preferentially collect at the bed top. This bed particle segregation occurs at around $U_g = 2$ m s^{-1} and this velocity increases with an increase in H. However, visual observations revealed that the degree of segregation was not dependent on time and it reached a steady state for each value of U_g and H.

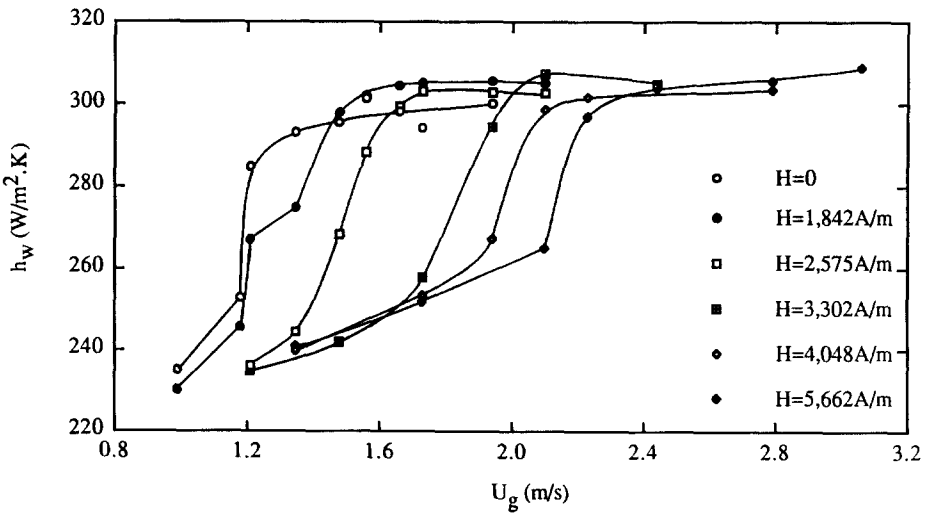

Fig. 6. Variation of h_w with increasing U_g and H for the iron bed.

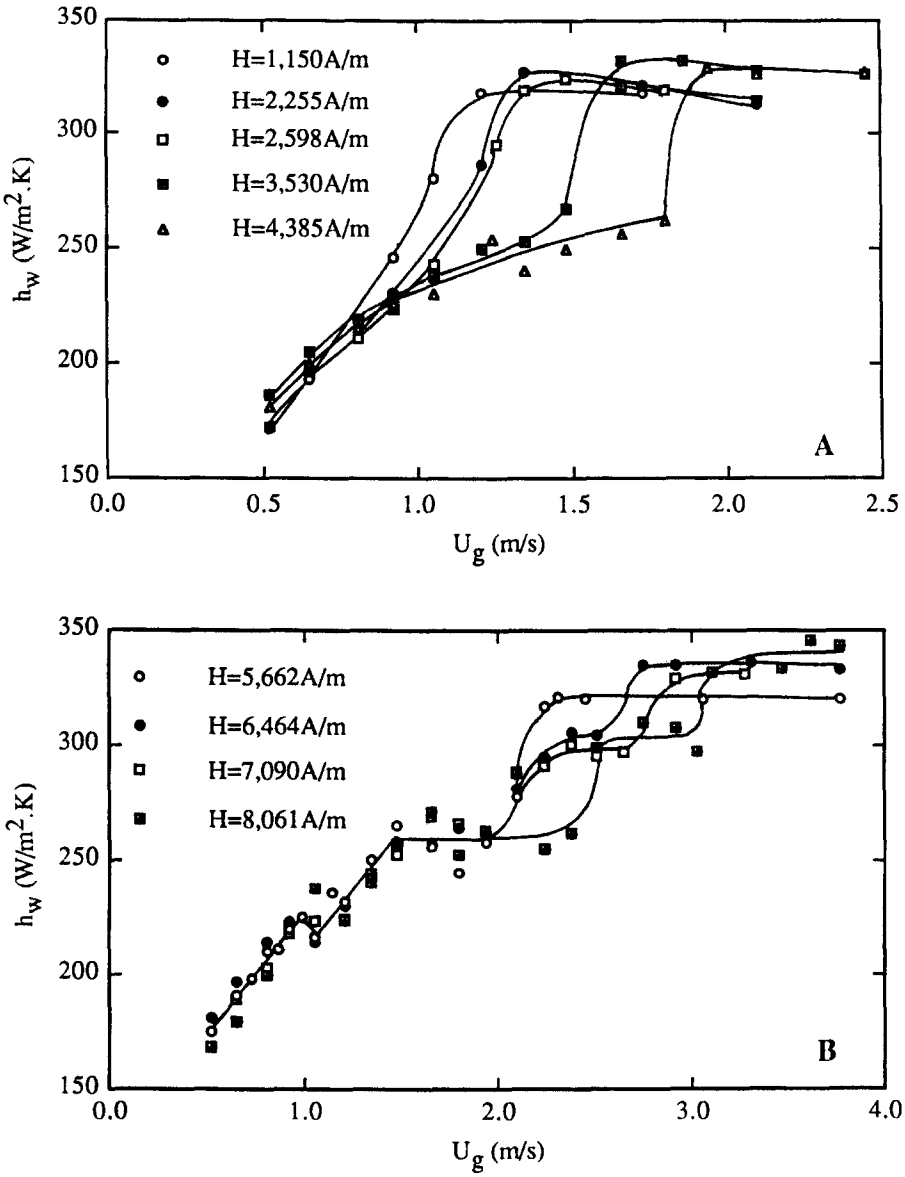

Fig. 7. Variation of h_w with increasing U_g and H for the admixture bed.

However, this nonmagnetic particle movement and their relatively greater mobility than magnetic particles enhances heat-transfer rate and is responsible for the characteristic difference in the h_w values in Fig. 7(a, b). In the latter case, before U_{mb} a jump in h_w values is the result of this bed segregation associated particle movement.

Ganzha *et al.* [14] proposed a mechanistic theory for large particle fluidized beds and showed that Nu is composed of conductive and convective terms such that

$$Nu = 8.95(1-\varepsilon)^{2/3} + CRe^{0.8}Pr^{0.43}(1-\varepsilon)^{0.133}\varepsilon^{-0.8}. \quad (8)$$

Saxena *et al.* [3] related C to the powder classification scheme of Saxena and Ganzha [15]. For the present bed powder and for the U_g range between U_{mf} and U_{mb}, $C = 0.085$ [3]. Further, Ganzha [16] showed that for gas–solid systems including particles of high thermal conductivity 8.95 should be replaced by 8.5 k_{gp} where

$$k_{gp} = \frac{1}{3.4(k_g/k_p)+0.94}. \quad (9)$$

Equation (8) finally becomes

$$Nu = 8.5k_{gp}(1-\varepsilon)^{2/3} + 0.085Re^{0.8}Pr^{0.43}(1-\varepsilon)^{0.133}\varepsilon^{-0.8}. \quad (10)$$

A mean value of 0.5 is assigned to ε in view of its small variation in the MSB regime. h_w data for this regime is only considered here in view of the lack of reliable

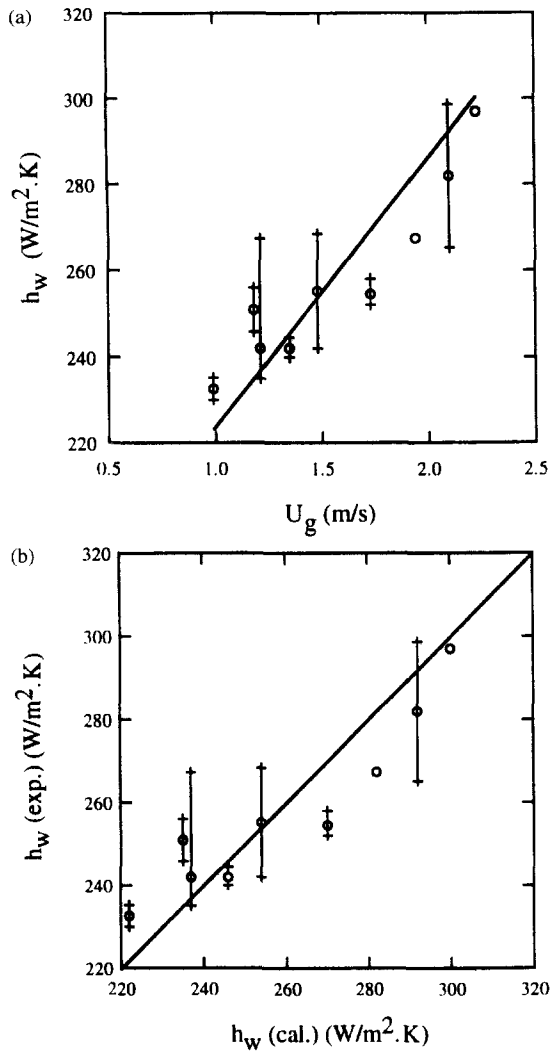

Fig. 8. (a) Variation of experimental h_w with U_g and comparison with theory for the iron bed; (b) comparison of the experimental and calculated h_w values for the iron bed.

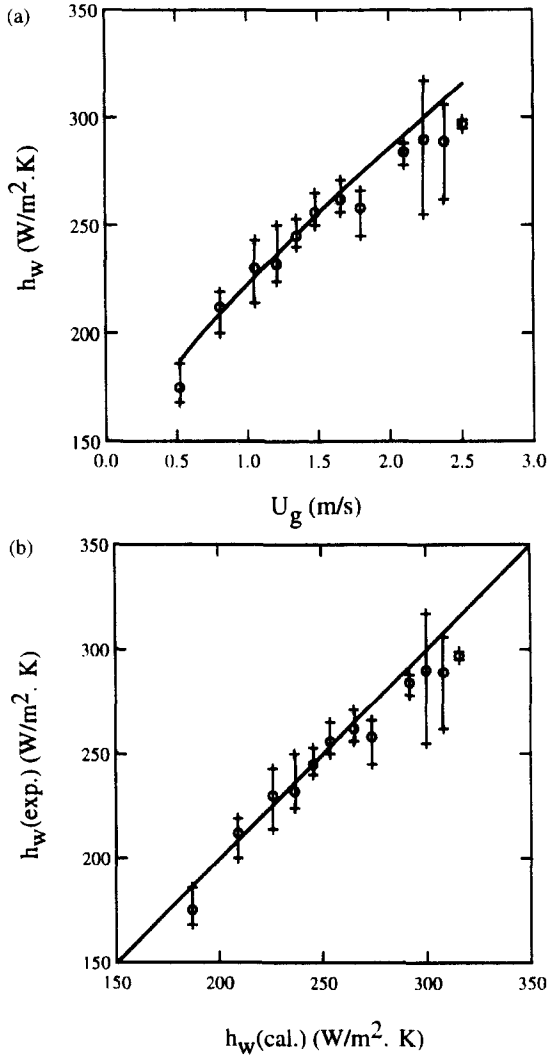

Fig. 9. (a) Variation of experimental h_w with U_g and comparison with theory for the admixture bed; (b) comparison of the experimental and calculated h_w values for the admixture bed.

ε data in the fluidized-bed regime. With this simplification, equation (10) becomes for the present case of air and iron/sand system

$$Nu = (h_w d_p/k_g) = 0.116 Re^{0.8} + 5.67. \quad (11)$$

In Fig. 8(a) are shown plotted h_w experimental values as a function of U_g for pure iron bed in the fixed bed and MSB regimes. Each data point is the average of h_w values for all H at that value of U_g. Corresponding computed values of h_w form equation (11) are also shown in Fig. 8(a) by continuous line. The agreement between calculated and average experimental h_w values is considered good as the deviations are even smaller than the differences in the experimental h_w values. The large scatter in experimental h_w values is due to the uncertainty in establishing the boundaries of MSB and MSFB regimes. In Fig. 8(b), an explicit comparison of calculated and experimental h_w values is presented and it is clear that the theory presented here is reliable for prediction purposes.

In Fig. 9 data similar to Fig. 8 are presented except these refer to an admixture of iron and sand particles. The agreement for admixture bed is also very good as for pure iron bed and this validates the prediction potential of equation (11) for admixtures of magnetic and nonmagnetic particles. k_p is taken as the mean for the values of iron and sand particles. k_{gp} is not very sensitive to k_p value as k_p is much larger than k_g.

CONCLUSIONS

The hydrodynamic and heat-transfer investigations conducted for magnetofluidized beds of iron and an admixture of iron and sand particles over an extended range of external magnetic-field intensity and air flu-

idizing velocity have revealed a number of interesting conclusions which are summarized below.

(a) The experimental superficial minimum bubbling gas velocities both for the iron bed and the admixture bed is found to increase with an increase in H and for the latter bed also with an increase in X_M. The observed dependence of U_{mb} on operating and system parameters for both the beds is well represented by a single correlation of equation (4). U_{mb} is found to be dependent on U_{mf}, Ar and E_R for a given gas–solid system. The new characteristic potential energy density ratio parameter E_R contains the dependence of U_{mb} on H and X_M.

(b) For the admixture bed, the gross behavior of ε and its variation with U_g is not capable of reflecting the changes in bed structure, particularly the separation of magnetic and nonmagnetic particles. Local or sectional bed voidage measurements can reveal more effectively the changes in bed characteristics as the bed undergoes structural changes as a result of segregation of bed particles. MSB and MSFB investigations when supplemented with such details as mentioned above can characterize them more effectively.

(c) h_w variation with U_g under the influence of H is well represented mechanistically if considered as being comprising of three distinct regimes. The fixed-bed regime ($U_g < U_{mf}$) is characterized with a slow increase in h_w with an increase in U_g. The stabilized-bed regime ($U_{mf} \leqslant U_g \leqslant U_{mb}$) exhibits a comparatively involved variation of h_w with an increase in U_g. This is well explained by a particle convective component which is due to limited particle movement resulting from particle agitation and arrangement, and is more easily understood for a powder having a size range. The other component contributing to h_w results from gas convection which undergoes changes as ε changes due to particle arrangement. The partially stabilized fluidized-bed regime ($U_g > U_{mb}$) involves bubbling and increasing particle movement and back mixing. h_w rapidly increases and acquires a constant value at sufficiently large U_g values. This behavior is somewhat similar to that of an unstabilized bubbling fluidized bed. These three regimes are relatively distinctly realized as H is increased. The h_w variation with U_g gets a bit complicated for admixture beds which may undergo partial segregation at higher H and U_g values.

(d) The experimental h_w data for the pure iron and an admixture bed of iron and sand particles in the magnetically stabilized-bed regime is adequately represented by a correlation developed by the authors earlier for fluidized beds and after an appropriate modification for the high thermal conductivity of bed particles.

REFERENCES

1. Sonolikar, R. L., Magneto-fluidized beds. In *Transport in Fluidized Particle Systems*, eds L. K. Doraiswamy and A. S. Mujumdar, 1989, pp. 359–422.
2. Liu, Y. A., Hamby, R. K. and Colberg, R. D., Fundamental and practical developments of magnetofluidized beds: a review. *Powder Technology*, 1991, **64**, 3–41.
3. Saxena, S. C., Ganzha, V. L., Rahman, S. H. and Dolidovich, A. F., Heat transfer and relevant characteristics of magnetofluidized beds. In *Advances in Heat Transfer*, eds J. P. Hartnett and T. F. Irvine Jr, Vol. 25, 1994, pp. 151–249.
4. Bologa, M. K. and Syutkin, S. V., The influence of a magnetic field on heat transfer in a fluidized bed. *Electrochemistry and Industrial Processing and Biology*, 1976, **6**, 61–66.
5. Neff, J. J. and Rubinsky, B., The effect of a magnetic field in the heat transfer characteristics of an air fluidized bed of ferromagnetic particles. *International Journal of Heat and Mass Transfer*, 1983, **26**(12), 1885–1889.
6. Arnaldos, J., Puigjaner, L. and Casal, J., Heat and mass transfer in magnetically stabilized fluidized beds. *Proceedings of Fifth Engineering Foundation Conference on Fluidization, Fluidization V*, eds K. Ostergaard and A. Sorensen, 1989, pp. 425–432.
7. Qian, R. Z. and Saxena, S. C., Heat transfer from an immersed surface in a magnetofluidized bed. *International Communication of Heat and Mass Transfer*, 1993, **20**, 859–869.
8. Saxena, S. C. and Dewan, S. S., Heat transfer from a horizontal tube in a magnetofluidized bed. *International Communication of Heat and Mass Transfer*, 1996, **23**(5), 655–664.
9. Wu, W. Y., Navada, A. and Saxena, S. C., Hydrodynamic characteristics of a magnetically stabilized air-fluidized bed of an admixture of magnetic and nonmagnetic particles. *Powder Technology*, 1997, **90**, 39–46.
10. Wu, W. Y., Smith, K. L. and Saxena, S. C., Hydrodynamic characteristics of a magnetically stabilized air-fluidized bed of an admixture of magnetic (10 mass %) and nonmagnetic (90 mass %) particles. *Powder Technology* (in press).
11. Saxena, S. C. and Shrivastava, S., Some hydrodynamic investigations of a magnetically stabilized air-fluidized bed of ferromagnetic particles. *Powder Technology*, 1991, **64**, 57–67.
12. Ganzha, V. L. and Saxena, S. C., A model for the calculation of minimum bubbling velocity of a magnetically stabilized admixture bed (to be published).
13. Agbim, J. A., Nienow, A. W. and Rowe, P. N., Interparticle forces that suppress bubbling in gas fluidized beds. *Chemical Engineering Science*, 1971, **26**, 1293–1294.
14. Ganzha, V. L., Upadyay, S. N. and Saxena, S. C., A mechanistic theory for heat transfer between fluidized beds of large particles and immersed surfaces. *International Journal of Heat and Mass Transfer*, 1982, **25**(10), 1531–1540.
15. Saxena, S. C. and Ganzha, V. L., Heat transfer to immersed surfaces in gas-fluidized beds of large particles and powder characterization. *Powder Technology*, 1984, **39**, 199–208.
16. Ganzha, V. L., Heat and mass transfer in dispersed media with two-phase flow. D.Sc. thesis, Luikov Institute of Heat and Mass Transfer of the Academy of Sciences of Belarus, Minsk, 1992.